Digital holographic microscopy reveals prey-induced changes in swimming behavior of predatory dinoflagellates

Jian Sheng*, Edwin Malkiel*, Joseph Katz*†, Jason Adolf‡, Robert Belas‡, and Allen R. Place‡

*Department of Mechanical Engineering, The Johns Hopkins University, 3400 North Charles Street, Baltimore, MD 21218; and ‡Center of Marine Biotechnology, University of Maryland Biotechnology Institute, 701 East Pratt Street, Baltimore, MD 21202

Edited by J. Woodland Hastings, Harvard University, Cambridge, MA, and approved September 6, 2007 (received for review May 17, 2007)

The shallow depth of field of conventional microscopy hampers analyses of 3D swimming behavior of fast dinoflagellates, whose motility influences macroassemblages of these cells into often-observed dense "blooms." The present analysis of cinematic digital holographic microscopy data enables simultaneous tracking and characterization of swimming of thousands of cells within dense suspensions. We focus on *Karlodinium veneficum* and *Pfiesteria piscicida*, mixotrophic and heterotrophic dinoflagellates, respectively, and their preys. Nearest-neighbor distance analysis shows that predator and prey cells are randomly distributed relative to themselves, but, in mixed culture, each predator clusters around its respective prey. Both dinoflagellate species exhibit complex highly variable swimming behavior as characterized by radius and pitch of helical swimming trajectories and by translational and angular velocity. *K. veneficum* moves in both left- and right-hand helices, whereas *P. piscicida* swims only in right-hand helices. When presented with its prey (*Storeatula major*), the slower *K. veneficum* reduces its velocity, radius, and pitch but increases its angular velocity, changes that reduce its hydrodynamic signature while still scanning its environment as "a spinning antenna." Conversely, the faster *P. piscicida* increases its speed, radius, and angular velocity but slightly reduces its pitch when exposed to prey (*Rhodomonas* sp.), suggesting the preferred predation tactics of an "active hunter."

The swimming behavior of dinoflagellates, biflagellated planktonic protists that are sometimes associated with harmful algal blooms or "red tides" (1), is vital to their success in aquatic ecosystems (2). Predation, which involves complex microbial interactions, is an important facet of the behavior of heterotrophic and mixotrophic (combining phototrophic and heterotrophic nutrition) dinoflagellates (3). Dinoflagellates typically move in helical trajectories (4, 5), which may help them in detecting nutrient gradients (6), although little is known about how differences in species or environment (i.e., resource availability) affect their swimming characteristics. However, evidence suggests that certain dinoflagellates adapt swimming strategy that increases their encounter rate with prey as the quarry concentration decreases (7).

Being limited by the shallow depth of field of conventional microscopy, most studies of dinoflagellates' swimming have been performed in thin containers, where "wall effects" are likely to affect behavior. Triggering of imaging systems as subjects cross in-focus planes or 3D traversing systems that follow organisms provide only limited solutions to this problem. The tendency of dinoflagellates to cluster together in dense suspensions further complicates measurements of behavior of individuals in their natural setting. In this study, we use high-speed cinematic digital holographic microscopy, as described in *Materials and Methods*, to overcome these challenges. Ensuing analysis provides simultaneous data on 3D swimming behavior of thousands of organisms in space and time within dense suspensions of 50,000–100,000 cells per ml that have substantial depth (3 mm, ≈300 cell lengths). Obtaining data on behavior of 500–1,000 individuals in a sample of dinoflagellates alone and comparing its statistics to those occurring in mixed cultures of dinoflagellate predators and their cryptophytes prey enables us to quantify the substantial species-dependent change in behavior of predatory dinoflagellates in the presence of prey.

As a representative for heterotrophic dinoflagellates, we measure the swimming characteristics of *Pfiesteria piscicida*, a relatively fast (8) 5- to 20-μm voracious grazer (9) that is widely distributed in temperate-subtropical estuarine waters (10, 11) and has been linked to major fish kills, fish lesions, and adverse human health impacts (12–15). As a representative of mixotrophic dinoflagellates (i.e., those that graze prey and perform photosynthesis), we examine the swimming of *Karlodinium veneficum*, a slower, 10- to 15-μm cell with a worldwide distribution (16, 17) that has been associated with fish kills (18–20). *P. piscicida* can consume algal prey (9) two to three times faster than *K. veneficum* (21). Although *P. piscicida* depends on prey consumption for survival, *K. veneficum* does not. The response to prey is examined for both species by introducing cryptophytes (unicellular flagellated algae) into the media. We show that both dinoflagellates regularly perform complex swimming maneuvers, but their responses to introduction of prey are diametrically different.

Results and Discussion

Gallery of Motion of Individual Cells. In this section, we present samples of the characteristic trajectories of the dinoflagellates demonstrating the variability in raw data and the ability of digital holographic microscopy to capture the shape and 3D motions of multiple particles simultaneously in densely populated samples. Spatial resolution is 0.975 μm in directions parallel to the imaging plane and 2 μm in depth direction. Temporal resolution, as determined by acquisition rate, is 120 Hz. Fig. 1*a* is a typical 3D trajectory of a *K. veneficum* with velocity magnitude color-coded, shown along with selected (1 in 20) in-focus images of the cell. In one of the frames, the organism is located near another out-of-focus particle. Additional *K. veneficum* tracks are presented in Fig. 1*b*. The complexity of movement is self-evident, displaying varying pitch and radius of helices, as defined in Fig. 1*a*, and velocity magnitudes, which are typically in the 20–90 μm/s range. Although most helices are right-handed, this organism frequently switches to left-handed helices. Fig. 1*c* shows a sample trajectory of *K. veneficum* (red) moving in unison with its prey, *Storeatula major* (blue), the latter being distinguished from predator by its smaller size (6–8 μm) and ellipsoidal shape. Selected images of predator and prey

Author contributions: J.S., E.M., and J.K. designed research; J.S. performed research; E.M., J.A., R.B., and A.R.P. contributed new reagents/analytic tools; J.S., J.K., J.A., R.B., and A.R.P. analyzed data; and J.S., J.K., J.A., R.B., and A.R.P. wrote the paper.

The authors declare no conflict of interest.

This article is a PNAS Direct Submission.

Abbreviations: NND, nearest-neighbor distance; PDF, probability distribution function.

†To whom correspondence should be addressed. E-mail: katz@jhu.edu.

This article contains supporting information online at www.pnas.org/cgi/content/full/0704658104/DC1.

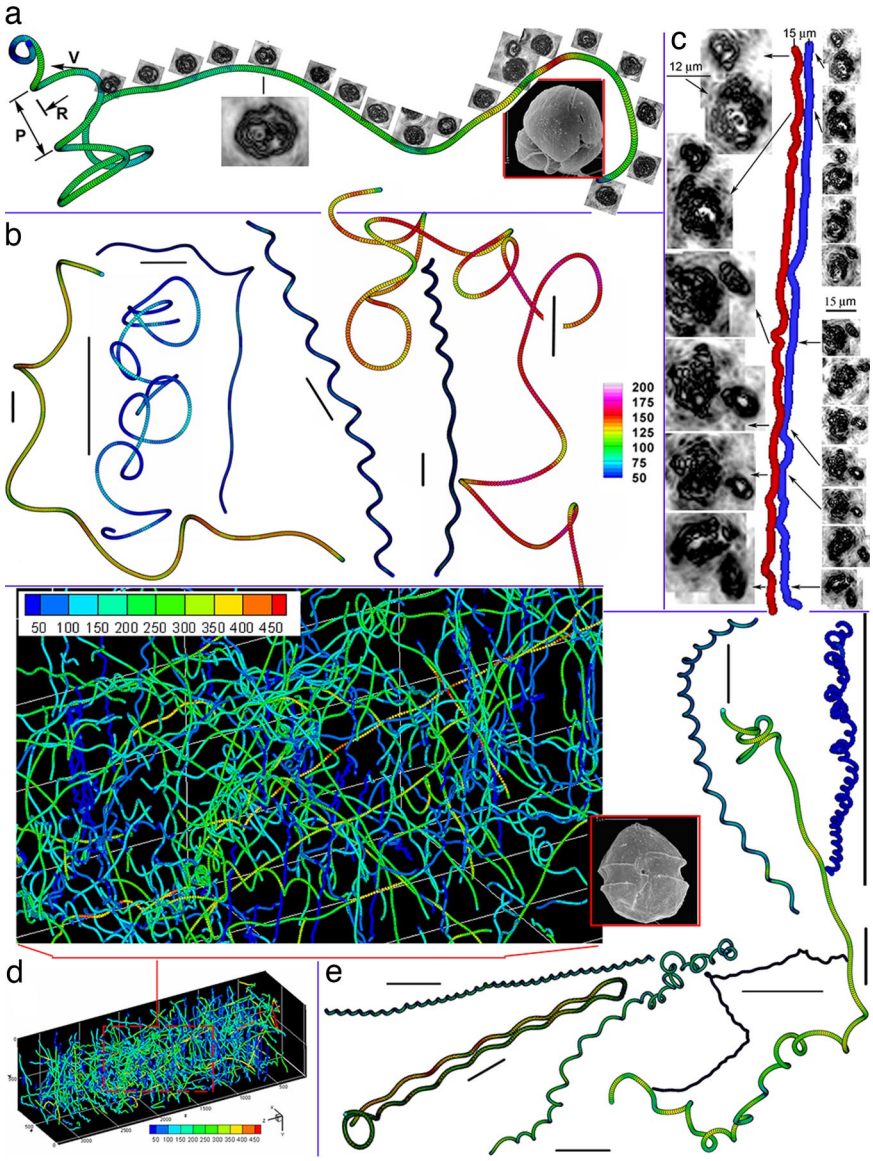

Fig. 1. Gallery of dinoflagellate motion. (*a*) A 3D trajectory of *K. veneficum*, color-coded with cell swimming velocity, superimposed with in-focus images sampled at every 40 time steps (0.33 s). (*Insets*) SEM and reconstructed image of *K. veneficum*. (*b*) Sample characteristic trajectories of *K. veneficum cells*. (Scale bars: 50 μm.) (*c*) Sample trajectories of *K. veneficum* and *S. major* moving in unison. To the right of trajectories are shown selected in-focus images of predator and prey cells, with arrows indicating timing of image. To the left of the trajectories are shown some of the images magnified $\times 4$ with arrows indicating corresponding timing. (*d*) The 3-mm-deep sample volume showing trajectories of *P. piscicida* before introduction of prey. (*Upper Inset*) Close-up of part of the sample volume, which is marked by red dash-dot line in *d*. (*e*) Samples characteristic tracks of *P. piscicida* cells with velocity magnitude color-coded. (Scale bars:100 μm.) (*Inset*) SEM of *P. piscicida*. [SEMs reproduced with permission (Copyright 1995, Florida Wildlife Conservation Commission).]

cells are shown to the right of the trajectories, with arrows indicating the timing of each image. To provide clearer details, some images are magnified $\times 4$ and shown to the left of the trajectories.

Fig. 1*d* presents an overall view of an entire $0.8 \times 0.8 \times 3.0$ mm volume (the latter is depth), this time containing *P. piscicida* alone, along with a magnified section of this sample. All four raw databases of this study have similar "spaghetti"-like patterns with varying directions, scales, and velocity. Selected characteristic trajectories of individuals, from this sample and from the one with prey, are presented in Fig. 1*e*. Clearly, the velocity of *P. piscicida* is higher than that of *K. veneficum*, reaching 380 μm/s, and it varies substantially over short distances. Essentially, all of the *P. piscicida* trajectories are right-handed, but pitch and radius change significantly along the same trajectory. Clearly, helical motion with substantial maneuvering capability is the dominant swimming mode of both dinoflagellates. As discussed below, the velocity, radius, and pitch of helices are species-dependent and altered by presence of prey.

Statistics and Analysis of Swimming Behavior of Dinoflagellates. Dynamics of dinoflagellate swimming can be characterized by translational velocity (V), pitch (P), and radius (R) of helices and angular velocity, $\omega = 2\pi/\mathrm{T} = V/(R^2 + P^2)^{1/2}$. Any three of these parameters fully quantifies the motion, including progress along the helical centerline (directed motion), which is obtained from $P{\cdot}\omega/2\pi$. Joint probability distribution functions (PDFs) involving these parameters, highlighting swimming behavior of *K. veneficum* alone (before introducing prey), are presented in Fig. 2 *a* and *e*, and results for *P. piscicida* alone are shown in Fig. 2 *c* and *g*. Here, a negative radius indicates a left-handed helical trajectory. Mean values and

Table 1. Mean statistics of velocity, radius, pitch, angular velocity, and acceleration of the organisms

Culture	Velocity, $\langle V\rangle \pm \sigma_V$, μm/s	Helix radius, $\langle R\rangle \pm \sigma_R$, μm	Pitch of a helix, $\langle P\rangle \pm \sigma_P$, μm	Angular velocity, $\langle\omega\rangle \pm \sigma_\omega$, rad/s	Acceleration, $\langle a\rangle \pm \sigma_a$, mm/s^2
K. veneficum (control)	80.9 ± 38.9	4.3 ± 8.4	61.6 ± 52.8	5.0 ± 2.7	(0.66 ± 0.72) × 10^4
K. veneficum (with prey)	37.8 ± 40.1	0.0 ± 6.2	35.2 ± 45.2	6.8 ± 3.8	(0.02 ± 0.0197) × 10^4
P. piscicida (control)	173.8 ± 83.0	9.6 ± 8.7	80.4 ± 70.4	7.0 ± 3.5	(0.68 ± 0.66) × 10^4
P. piscicida (with prey)	240.4 ± 112.6	11.4 ± 9.0	60.9 ± 60.9	11.7 ± 6.1	(1.25 ± 1.83) × 10^4
S. major (with predator)	61.3 ± 44.9	−0.7 ± 5.5	37.4 ± 49.0	7.2 ± 4.0	(1.76 ± 1.66) × 10^4
Rhodomonas sp. (with predator)	84.5 ± 26.6	0.0 ± 2.3	44.6 ± 56.5	3.0 ± 2.2	(2.24 ± 2.29) × 10^4

$\langle\rangle$ Indicates ensemble mean, and σ indicates the standard deviation.

standard deviations are provided in Table 1. Both dinoflagellates move in helical trajectories, in agreement with prior observations (5–9), with wide ranges of velocity, pitch, and radius. Although PDFs of velocity vs. radius are broad (Fig. 2 *a* and *c*), in both cases, velocity increases with radius. However, the mean velocity of the slower *K. veneficum* is <50% that of *P. piscicida*. The variability in *K. veneficum* velocity is also much lower, as evidenced by corresponding σ_V (Table 1). The range of radii is similar (0–15 μm), but those of the *P. piscicida* helices are larger and always right-handed, whereas *K. veneficum* swim in left-handed trajectories 25% of the time. The mean pitch of *K. veneficum's* helix and its standard deviation are 25% smaller than those of *P. piscicida's*. Mean angular velocity magnitude of *P. piscicida* and its variability are 25% higher than those of *K. veneficum*.

Substantial changes in all PDFs of swimming parameters of both dinoflagellates occur in response to prey but trends differ. In the presence of *S. major* (Fig. 2 *b* and *f* and Table 1), the mean and variance of velocity, radius, and pitch of *K. veneficum* decrease. Furthermore, the skewed radius–velocity joint PDF without prey (Fig. 2*a*), which indicates preferred right-handed helices and velocity increasing with radius, becomes symmetric in the presence of prey (Fig. 2*b*), with smaller radii and almost equal chances of being right or left-handed helices. The bimodal diverging PDF with positive and negative radii indicates that velocity still increases with radius. The radius–pitch PDF also becomes more symmetric (Fig. 2*f*) with branches extending to small positive and negative radii.

Exposure to *Rhodomonas* (Fig. 2 *d* and *h* and Table 1) also causes changes in velocity, radius, and pitch of *P. piscicida* movement. The single-mode in joint PDFs of the organism alone (Fig. 2 *c* and *g*) changes to bimodal distributions (Fig. 2 *d* and *h*). However, >80% of the population significantly increases its velocity and radius but decreases its pitch. Although the overall mean velocity increases only by 38% (Table 1), in part because of low speed contribution, the most probable velocity (PDF peak) doubles, from 160 μm/s with no prey to 320 μm/s (Fig. 2 *c* and *d*). Similarly, the mean radius increases by 20%, but the most probable value increases from 10 to 15 μm. Even after introducing prey, essentially all *P. piscicida* cells move in right-hand helices. Meanwhile, the mean pitch decreases by 25% (Fig. 2 *g* and *h*).

PDFs of angular velocities for both organisms are shown in Fig. 3. In the case of *P. piscicida*, introduction of prey substantially expands the distribution of ω, resulting in 67% increase in mean value and 75% increase in standard deviation (Table 1). Clearly, in the presence of prey, *P. piscicida* moves faster in a larger radius and with a higher and more variable angular velocity. Unlike the reduction in translational velocity of *K. veneficum* in the presence of prey, the angular velocity increases. However, the PDFs (Fig. 3) show that the mode remains at 4 rad/s, but the mean value increases slightly since the distribution broadens, causing a 40% increase in σ_ω (Table 1). In an attempt to elucidate this trend, we performed conditional sampling of radius and pitch based on angular velocity. A sample, conditioned on $\omega > 7$, is shown as an inset in Fig. 3. The

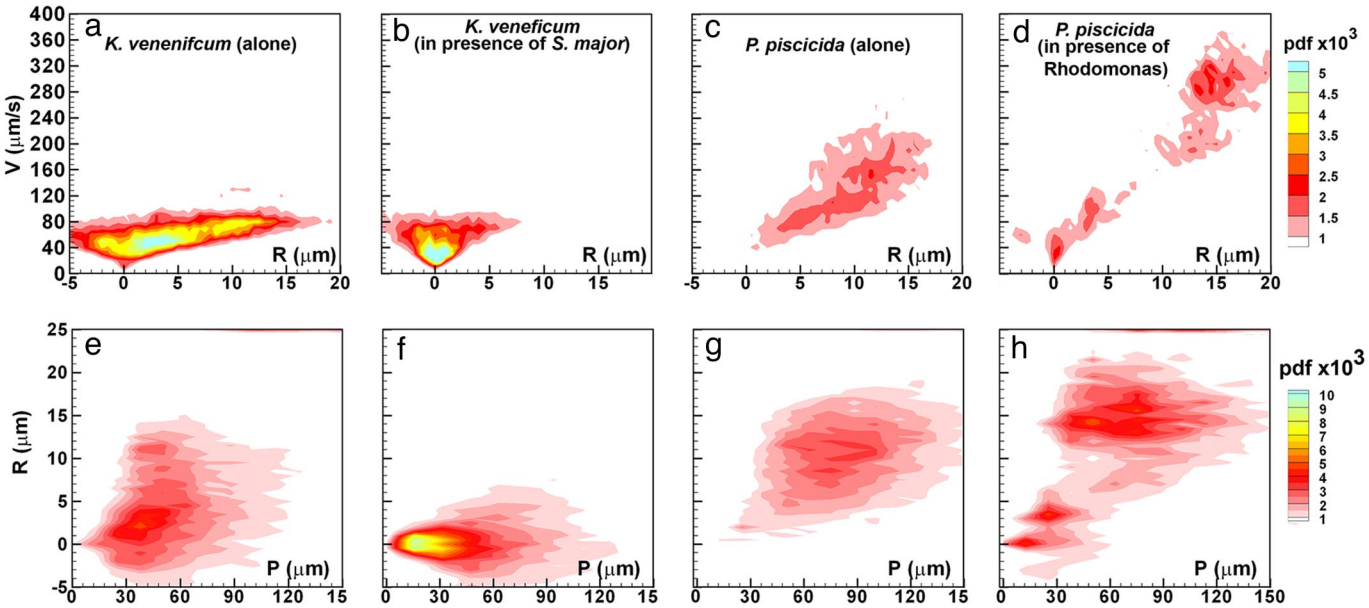

Fig. 2. Joint PDFs of swimming behavior characterized by velocity (*V*), radius (*R*), and pitch (*P*) of helices. (*a–d*) Joint PDFs of *V* and *R*. (*e–h*) Joint pdfs of *R* and *P*. Each column represents a different experimental condition. (*a* and *e*) *K. veneficum* alone. (*b* and *f*) *K. veneficum–S. major* mixture. (*c* and *g*) *P. piscicida* alone. (*d* and *h*) *P. piscicida–Rhodomonas* sp. mixture.

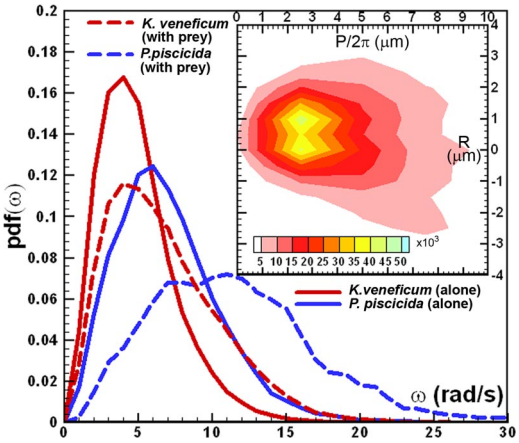

Fig. 3. PDFs of angular velocities of predators with and without preys. (*Inset*) Conditionally sampled joint PDF of swimming radius and pitch of *K. veneficum* in the presence of prey, conditioned on $\omega > 7$ rad/s.

peak is located at a radius of ≈1 μm and pitch of ≈12 μm, significantly lower than the corresponding overall values, indicating that elevated angular velocity is associated with small radius and pitch. *K. veneficum* seems to slow down while increasing the scanning frequency of its surrounding. Changes to the mean acceleration and its variance (Table 1), which indicates variability in motion, also demonstrate the different responses to prey. In suspensions with predators alone, the mean accelerations of both predators are very similar. After introducing prey, the acceleration of *P. piscicida* increases by 83%, whereas the acceleration of *K. veneficum* diminishes, indicating a slow nonvarying translation.

The very different responses of dinoflagellate predators of similar sizes to introduction of prey indicate distinctly different "predation strategies." The slower, less motile *K. veneficum*, when exposed to prey that swim at a comparable velocity (Table 1), substantially reduces its linear motion but increases its rotation rate. Conversely, *P. piscicida*, which is faster than its prey, greatly increases its linear motion and rotation rate. These dissimilar behaviors are most likely associated with physiological differences between organisms. *P. piscicida* uses a peduncle, an extensible mouth-like feeding appendage, to capture prey directly, and seems to adopt an "active hunter's" tactics of chasing prey (10, 22). Conversely, *K. veneficum* seems to use "ambush tactics" and then extends a tether (capture filament) to capture and haul in its quarry (21, 23). The higher velocity and radius in the absence of food may represent a "search mode," aimed at increasing the volume being scanned. By slowing down, *K. veneficum* reduces its own hydrodynamic signature, possibly to camouflage its presence and decrease the likelihood of being detected by prey. However, in the Stokes flow low-Reynolds world ($Re \approx 0.001$) for self-propelled bodies (i.e., ignoring effect of gravity), the flow, induced by swimming, is proportional to velocity but decays faster than the distance squared (24, 25); i.e., the hydrodynamic signature of such motion is quite local. One may also speculate that increasing its angular velocity when the radius is small helps the *K. veneficum* detect prey by operating as a "fast spinning antenna."

Structure of a Suspension: Nearest-Neighbor Distance (NND). The cell suspension structure and location of an organism relative to others can be characterized based on the NND among individuals of the same species and between predator and prey (26). The NNDs are calculated from 3D loci of all dinoflagellates and prey at each given moment. PDFs of ensemble averaged NNDs with and without prey are presented in Fig. 4, each compared with a random distribution (dash-dot lines) at the same concentration. Deviation from a random distribution shows whether the likely position of an organism within a suspension is affected by presence of other particles.

Fig. 4 *a* and *c* compare NNDs of control samples, i.e., those without prey, to those for all particles in samples with prey. Data indicate that both control populations have random distributions (null hypothesis) with confidence levels >94% (*z*-scores of −0.87 for *K. veneficum* and −0.91 for *P. piscicida*). At a concentration of 50,000–100,000 cells per ml, both *K. veneficum* and *P. piscicida* appear to be oblivious to other cells of the same species. A likely contributor to this trend is the rapid decay of swimming induced flow with distance (24, 25). This does not imply that there is no momentary reaction to contact or proximity between cells, e.g., a brief increase in *K. veneficum* velocity when it comes close to another cell (Fig. 1*a*). However, such interactions have little effect on NND statistics, suggesting that cell–cell interactions seem to be short-lived and localized, e.g., altering trajectories to prevent collision. They have little effect on how cells are arranged in a

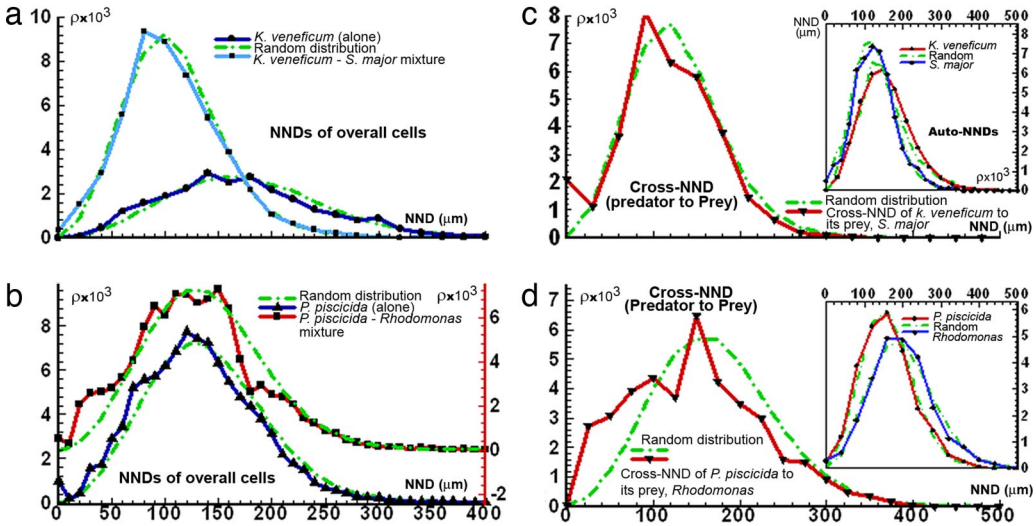

Fig. 4. Probability density functions of NND (solid lines) superimposed with those obtained for random distributions (dash-dot lines) at the corresponding cell concentrations. (*a*) Overall NND of *K. veneficum* alone and *K. veneficum–S. major* mixture. (*b*) Overall NNDs of *P. piscicida* alone and of *P. piscicida–Rhodomonas* sp. mixture. (*c*) Cross-NND between predator and prey cells in *K. veneficum–S. major* mixture. (*Inset*) PDFs of auto-NNDs between predator and prey cells themselves. (*d*) Cross-NND between predator and prey cells in the *P. piscicida–Rhodomonas* mixture. (*Inset*) Auto-NNDs between predator and prey cells themselves.

Table 2. Experimental conditions and characteristics of organisms

Culture	Concentration, cells per ml	Prey/predator ratio	Cells examined, *n*	Species	Length, μm	Width, μm
K. veneficum (alone)	50,000	0	412	*K. veneficum*	12–15	8–10
K. veneficum + *S. major*	150,000	2:1	991	*S. major*	8–10	6–8
P. piscicida (alone)	100,000	0	763	*P. piscicida*	8–10	6–8
P. piscicida + *Rhodomonas* sp.	100,000	1:1	784	*Rhodomonas* sp.	6–8	6–8

suspension. Conditional samplings of velocity, acceleration, and direction of swimming as a function of distance between cells (data not shown) do not display significant trends, showing no evidence that local interactions affect the statistics of motion.

In the *K. veneficum* data (Fig. 4*a*), a higher prey concentration (Table 2) decreases the mean NND between particles. In the *P. piscicida* case (Fig. 4*c*), prey and predator cultures have the same concentration, i.e., the mean NND does not change when predator is mixed with prey. In both cases, as preys are introduced, the NNDs cease to be random, showing clear evidence of clustering with confidence level >99% (*z*-scores of −1.87 for the *K. veneficum–S. major* mixture and −2.98 for the *Pfiesteria–Rhodomonas* mixture).

Further understanding comes from measuring the auto-NNDs, i.e., the distances among predator and prey themselves, and cross-NNDs, the distance from predator to prey (Fig. 4 *b* and *d*). All four auto-NNDs are nearly randomly distributed, i.e., there is no evidence of clustering among organisms of the same species (*z*-scores of 0.67 and −0.51, respectively). Conversely, the cross-NNDs deviate substantially from random distributions. Two-tailed testing (27) shows 99.1% confidence in claiming clustering for the *K. veneficum–S. major* cross-NND and 99.99% in the *P. piscicida–Rhodomonas* case. Cleary, clustering in overall NNDs is caused by predators preferentially locating themselves near their prey.

In the *K. veneficum–S. major* mixture (Fig. 4*b*), clustering is manifested by a shift in the peak of the NND PDF from 115 to 95 μm, i.e., by approximately one cell length. Furthermore, there is a considerable increase in the number of predator cells that are located less than one body length (NND less than ≈15 μm) from their prey. As noted before, we have seen seven cases of *K. veneficum* and *S. major* moving in unison over the entire 13-s test period, in trajectories that do not involve helical motion. The distance between predator and prey remains almost constant, but their relative orientation varies (Fig. 1*c*). Because *K. veneficum* extends a capture filament to capture and haul in its prey in a process lasting ≈3 min (21, 23), it is possible we are observing part of the predation process.

The PDF peak of the *P. piscicida–Rhodomonas* mixture remains at the same distance, and clustering is manifested as a deficit compared with random distribution at NND ≈ 200 μm (≈25 liters) and augmentation at NND ≈ 30 μm, i.e., approximately four body lengths. Clustering causes a selective change in length scale, not a broad-spectrum reduction in the NND that would characterize the clustering of nonmotile particles in, e.g., turbulent flow (28). Namely, a significant fraction of the *P. piscicida* cells, originally located 15–25 cell lengths away from their prey, preferentially reduce their distance from prey to 0–12 body lengths. This targeted reduction also appears in the NND PDF of *K. veneficum–S. major* mixture, but it is less pronounced.

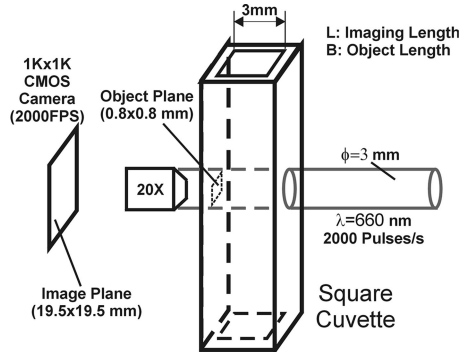

Fig. 5. Experimental setup of a digital holographic microscope and sample volume.

Conclusion

Holographic microscopy provides an unprecedented ability to measure cellular behavior and interactions among microorganisms in dense suspensions and analyze behavior in response to various stimuli, e.g., characterization of helical motion, showing that *K. veneficum* swims in both right and left-hand helices. Using detailed statistics obtained in dense suspensions, we demonstrate that dinoflagellates of similar size but with different swimming characteristics, speed in comparison to prey, and feeding strategies (peduncle vs. tow line) have substantially different responses to introduction of prey. The distance between organisms of the same species in dense suspensions, with or without prey, has a random distribution, but predators clearly cluster around prey.

The present analysis should extend further, e.g., to search for Levy Walk search strategy by following the procedures of Bartumeus *et al.* (7). On first glance, the present frequency spectra of time series of velocity components (data not shown) do not reveal a range with power law decay with increasing frequency. It seems that unlike the behavior of the dinoflagellate in (7) (*Oxyrrhis marina*), the scales of directed motion and those of helical trajectories in our study overlap, obscuring the spectral trends of directed motion. However, using the velocity component aligned with the helix axis to estimate directed motion, the spectral slopes of this component steepen (negative magnitude increases) when prey is introduced for both *K. veneficum* and *P. piscicida*, clearly in agreement with the study in ref. 7. Also, the previously mentioned conditional sampling was based solely on the distance between organisms, which does not reveal repeatable trends and appears to oversimplify the causes of the changes in behavior. For example, (*i*) even in Stokes flow, the induced motion by an organism is axisymmetric and not circumferentially uniform, i.e., it depends on direction and (*ii*) for Peclet numbers of 1–2.5 (VL/D; D is molecular diffusivity), the fore-aft chemical traces are not symmetric. Thus, one has to analyze response to cues based on the entire time history of motion, which is clearly achievable with the holographic microscopy data.

Materials and Methods

Materials. We use cultures of *P. piscicida* (CCMP 1830) and its prey, *Rhodomonas* sp. (CCMP 768), and *K. veneficum* (CCMP 2064) and it prey, *S. major*, in mid-log growth. *P. piscicida* and *Rhodomonas* sp. were maintained according to Alavi *et al.* (29). *K. veneficum* and *S. major* were grown and maintained in f/2 growth medium (36), 15 parts per thousand salinity, based on water from the Indian River Inlet, DE. Details on concentration and dimensions are summarized in Table 2. Measurements are performed at water temperatures of 23.5°C, between 11:50 a.m. and 12:35 p.m., with background light on.

Setup and Data Acquisition. The optical setup is illustrated in Fig. 5. Samples are placed in a glass cuvette with inner dimensions of 3 × 3 × 40 mm. Large dimensions in comparison to organism size ensure that cells are less likely to be influenced by boundaries in comparison with microscopic slides. Behavior is studied by using in-line cinematic digital holographic microscopy, which enables simultaneous recoding of thousands of particle traces located within a dense volume (30). Other approaches to digital holographic microscopy are described in refs. 31 and 32. Our process consists of illuminating the cuvette with a collimated, spatially filtered, pulsed ND:YLF laser beam (660-nm wavelength) and recording the interference pattern in a plane located 100 μm away from the inner wall of the cuvette. Using a 20× objective lens, the hologram is magnified and recorded for 13 s at 120 frames per second by a CMOS camera with 1,024 × 1,024 pixels, with a maximum acquisition rate of 2,000 frames per second at full frame and 19 × 19 μm pixels. Resolution is 0.975 μm per pixel in planes parallel to the hologram plane and ≈2 μm in depth. Image enhancement before reconstruction includes removal of time-invariant defects, e.g., scratches on windows, equalization to correct for laser intensity variations, subtraction of far-field to achieve spatial uniformity, and up-sampling to improve resolution. Numerical reconstruction (30, 33) performed at depth intervals of 10 μm over the 3-mm sample provides in-focus images of particles in each plane. Further details are provided in supporting information (SI) *Appendix*.

Data Analysis. Information on cell locations is extracted by using a hybrid, two-step autofocusing routine. First, 3D segmentation (30) is used to construct the 3D shape of each cell, followed by edge detection in-focus to determine its depth, where edges are sharpest. In-focus images of cells are stored along with the 3D location of their centroid and their cross-section areas and volumes. Depth resolution smaller than the distance between reconstructed planes is achieved by fitting a Gaussian curves to surface integrals of Laplacian derivatives in each plane (34). Tracking of cells in time utilizes size, shape, location, 3D correlations, velocity, and acceleration as criteria (see *SI Appendix*). Using differential geometry (35), helix parameters (Fig. 1) are calculated from the particle position vector, $\vec{r}(t)$, using

$$V(t) = |\dot{\vec{r}}(t)|;\ R = \frac{|\vec{e}_{\dot{r}} \times (\vec{e}_{\ddot{r}} \times \dot{\vec{e}}_{\ddot{r}}/|\dot{\vec{e}}_{\ddot{r}}|)|}{\sqrt{k^2 + \tau^2}};$$

$$P = \frac{\vec{e}_{\dot{r}} \cdot (\vec{e}_{\ddot{r}} \times \dot{\vec{e}}_{\ddot{r}}/|\dot{\vec{e}}_{\ddot{r}}|)}{\sqrt{k^2 + \tau^2}};\ |\omega| = V(t)\sqrt{k^2 + \tau^2};$$

$$k = |\dot{\vec{r}} \times \dddot{\vec{r}}|/\dot{\vec{r}}^3;\ \tau = \dot{\vec{r}} \cdot (\ddot{\vec{r}} \times \dddot{\vec{r}})/|\dot{\vec{r}} \times \dddot{\vec{r}}|^2,$$

where $\vec{e}(t)$ is a unit vector aligned with the vector indicated in subscript, the number of dots indicates order of time derivatives, k (as defined above) is the radius of curvature, and τ represents torsion. Associated uncertainties are ≈2.5% for 3D velocity and >5% for radius and pitch.

During analysis, predators are distinguished from prey based on shape and size. Besides automatic analysis based on measured dimensions, to gain confidence in the results, classification has been confirmed by manual examination of all in-focused images. The mean fluid velocity in the test section is calculated based on motion of particles moving in trajectories with zero radius, presumably immotile cells or other particles. It varies spatially because of existence of weak circulation, with maximum value of 25 μm/s, which varies little during each 13-s experiment. Local values are subtracted from velocity of each particle. Results do not show significant correlation between background fluid velocity and cell velocity relative to the fluid.

The Johns Hopkins University group was funded by National Science Foundation (NSF) Ecology and Oceanography of Harmful Algal Blooms Program Grant OCE-0402792 and the NSF Fluid Dynamics Program Grant CTS 0625571. Instrumentation was funded by NSF Major Research Instrumentation Grant CTS0079674. The Center of Marine Biotechnology group was supported by National Oceanic and Atmospheric Administration Coastal Oceans Program Grant NA04NOS4780276 (to A.R.P.), Centers for Disease Control and Prevention Grant U50/CCU 323376, the Maryland Department of Health and Mental Hygiene, and NSF Grant MCB-0446001 (to R.B.). This is contribution no. 07-175 of the Center of Marine Biotechnology and no. 243 from the Ecology and Oceanography of Harmful Algal Blooms Program.

1. Ramsdellm JS, Anderson DM, Glibert PM (2005) in *HARRNESS 2005, Harmful Algal Research and Response: A National Environmental Science Strategy 2005-2015* (Ecological Society of America, Washington, DC).
2. Kamykowski D (1995) *J Phycol* 31:200–208.
3. Graneli E, Carlsson P (1998) in *Physiological Ecology of Harmful Algal Blooms*, eds Anderson DM, Cembella AD, Hallegraeff GM (Springer, Berlin), pp 540–557.
4. Crenshaw HC, Ciampaglio CN, McHenry M (2000) *J Exp Biol* 203:961–982.
5. Fenchel T (2001) *Protist* 152:329–338.
6. Crenshaw HC (1996) *Amer Zool* 36:608–618.
7. Bartumeus F, Peters F, Pueyo S, Marrase C, Catalan J (2003) *Proc Natl Acad Sci USA* 100:12771–12775.
8. Burkholder JM, Glasgow HB (1997) *Limn Oceanogr* 42:1052–1075.
9. Lin SJ, Mulholland MR, Zhang H, Feinstein TN, Jochem FJ, Carpenter EJ (2004) *J Phycol* 40:1062–1073.
10. Parrow MW, Burkholder JM (2003) *J Phycol* 39:697–711.
11. Litaker RW, Steidinger KA, Mason PL, Landsberg JH, Shields JD, Reece KS, Haas LW, Vogelbein WK, Vandersea MW, Kibler SR, Tester PA (2005) *J Phycol* 41:643–651.
12. Burkholder JM, Glasgow HB, Hobbs CW (1995) *Mar Ecol Prog Ser* 124:43–61.
13. Grattan LM (1998) *MD Med J* 47:148–151.
14. Fleming LE, Easom J, Baden D, Rowan A, Levin B (1999) *Toxicol Pathol* 27:573–581.
15. Burkholder JM, Glasgow HB (2001) *Bioscience* 51:827–841.
16. Li AS, Stoecker DK, Coats DW (2000) *J Plank Res* 22:2105–2124.
17. Marshall HG (1999) *VA J Mar Sci* 50:281–285.
18. Terlizzi DE, Stoecker DK, Glibert PM (2000) in *AQUA 2000*, eds Flos R, Ressell L (European Aquaculture Society, Nice, France).
19. Kempton JW, Lewitus AJ, Deeds JR, Law JM, Wilde SB, Place AR (2002) *Harmful Algae* 1:233–241.
20. Deeds JR, Terlizzi DE, Adolf JE, Stoecker DK, Place AR (2002) *Harmful Algae* 1:169–189.
21. Li AS, Stoecker DK, Adolf JE (1999) *Aquat Microbial Ecol* 19:163–176.
22. Cancellieri PJ, Burkholder JM, Deamer-Melia NJ, Glasgow HB (2001) *J Exper Marine Biol Ecol* 264:29–45.
23. Adolf JE, Krupatkina D, Bachvaroff T, Place AR (2007) *Harmful Algae* 6:400–412.
24. Stone HA, Samuel ADT (1996) *Phys Rev Lett* 77:4102–4104.
25. Childress S, Koehl MAR, Miksis M (1987) *J Fluid Mech* 177:407–436.
26. Malkiel E, Abras JN, Widder EA, Katz J (2006) *J Plank Res* 28:149–170.
27. Walpole RE, Myers RH (1985) *Probability and Statistics for Engineers and Scientists* (Macmillan, New York).
28. Eaton JK, Fessler JR (1994) *Int J Multiph Flow* 20:169–209.
29. Alavi M, Miller T, Erlandson K, Schneider R, Belas R (2001) *Environ Microbiol* 3:380–396.
30. Sheng J, Malkiel E, Katz J (2006) *Appl Opt* 45:3893–3901.
31. Colomb T, Durr F, Cuche E, Marquet P, Limberger HG, Salathe RP, Depeursinge C (2005) *Appl Opt* 44:4461–4469.
32. Xu WB, Jericho MH, Meinertzhagen IA, Kreuzer HJ (2001) *Proc Natl Acad Sci* 98:11301–11305.
33. Malkiel E, Sheng J, Katz J, Strickler JR (2003) *J Exp Biol* 206:3657–3666.
34. Russ JC (2007) *The Image Processing Handbook* (CRC, Boca Raton, FL).
35. Berger M (1988) *Differential Geometry: Manifolds, Curves, and Surfaces* (Springer, New York).
36. Guillard RRL (1975) in *Culture of Marine Invertebrate Animals*, eds Smith WL, Chanley MH (Plenum, New York).